NeuroImage 215 (2020) 116810

Contents lists available at ScienceDirect

NeuroImage

journal homepage: www.elsevier.com/locate/neuroimage

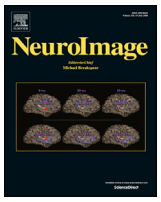

Electrically coupled inhibitory interneurons constrain long-range connectivity of cortical networks

Andrew W. Kraft [a], Anish Mitra [b], Zachary P. Rosenthal [c], Nico U.F. Dosenbach [c,d,e,g], Adam Q. Bauer [d], Abraham Z. Snyder [c,d], Marcus E. Raichle [c,d], Joseph P. Culver [d,e,f], Jin-Moo Lee [c,d,e,*]

[a] Department of Medicine, Brigham and Women's Hospital, Harvard Medical School, Boston, MA, USA
[b] Department of Psychiatry, Stanford University, Stanford, CA, USA
[c] Department of Neurology, Washington University, St. Louis, USA
[d] Department of Radiology, Washington University, St. Louis, USA
[e] Department of Biomedical Engineering, Washington University, St. Louis, USA
[f] Department of Physics, Washington University, St. Louis, USA
[g] Department of Program in Occupational Therapy, Washington University, St. Louis, USA

ARTICLE INFO

Keywords:
Connexin 36
Functional connectivity
Gap junction
Infra-slow activity
Neuroimaging

ABSTRACT

Spontaneous infra-slow brain activity (ISA) exhibits a high degree of temporal synchrony, or correlation, between distant brain regions. The spatial organization of ISA synchrony is not explained by anatomical connections alone, suggesting that active neural processes coordinate spontaneous activity. Inhibitory interneurons (IINs) form electrically coupled connections via the gap junction protein connexin 36 (Cx36) and networks of interconnected IINs are known to influence neural synchrony over short distances. However, the role of electrically coupled IIN networks in regulating spontaneous correlation over the entire brain is unknown. In this study, we performed OIS imaging on Cx36−/− mice to examine the role of this gap junction in ISA correlation across the entire cortex. We show that Cx36 deletion increased long-distance intra-hemispheric anti-correlation and inter-hemispheric correlation in spontaneous ISA. This suggests that electrically coupled IIN networks modulate ISA synchrony over long cortical distances.

1. Introduction

Even in the absence of environmental stimuli, the brain is spontaneously active over a wide frequency range (<0.01 Hz–600 Hz) (He et al., 2010). Infra-slow activity (ISA), defined as fluctuations in brain activity between 0.01 and 0.1 Hz, accounts for the vast majority of the power in spontaneous brain activity and occurs with precise spatiotemporal organization (Fox and Raichle, 2007). Previous work has shown that spontaneous ISA across distinct brain regions is temporally synchronous, and these patterns of correlated activity between regions define functionally connected networks (Biswal et al., 1995; Fox et al., 2005; Power et al., 2011). Correlation patterns (termed functional connectivity) in spontaneous activity are known to be stable within and between individuals (Laumann et al., 2015; Power et al., 2011). Moreover, these patterns are present with remarkable homology in non-human primates and rodents (Grayson et al., 2016; Stafford et al., 2014; Vincent et al., 2007; White et al., 2011). These findings suggest that resting state correlation patterns may be a fundamental feature of neurological function. Consistent with this, declining network correlation has been established as a common feature of neurological disease (Allen et al., 2007; Carter et al., 2010; Chase, 2014).

Despite intense scientific interest in functional connectivity, the molecular mechanisms responsible for creating these ISA correlation patterns remain poorly understood. While there is some overlap between anatomically connected regions and spontaneous ISA correlation, patterns in functionally connected systems are not explained by anatomical connections alone (Fox et al., 2005; Honey et al., 2009; Power et al., 2011; Vincent et al., 2007; Zhang et al., 2008). Furthermore, correlation strength varies widely between different anatomic networks for unknown reasons. Thus, ISA correlation is not merely a readout of structural connectivity. Biological mechanisms likely play a role in modulating brain activity to shape spontaneous activity correlation patterns.

* Corresponding author. Department of Neurology, Washington University School of Medicine, 660 S. Euclid, Campus Box 8111, Saint Louis, Missouri, 63110, USA.
E-mail address: leejm@wustl.edu (J.-M. Lee).

https://doi.org/10.1016/j.neuroimage.2020.116810
Received 15 October 2019; Received in revised form 11 March 2020; Accepted 24 March 2020
Available online 7 April 2020

Coordinated inhibitory neural activity may play a role in shaping functional connectivity. At higher frequencies, inhibitory activity is known to organize excitatory neural activity into well-defined rhythms (Buzsaki and Chrobak, 1995; Lytton and Sejnowski, 1991; Whittington et al., 1995). These rhythms emerge in part because inhibitory interneurons (IINs) form robust local networks via reciprocal connections with adjacent IINs, via both chemical and electrical synapses (Deans et al., 2001; Galarreta and Hestrin, 2002; Hormuzdi et al., 2001). Electrical synapses, or gap junctions, are formed by connexin proteins that create a "bridge" between cells that enables direct ion passage (Evans and Martin, 2002). Connexin 36 (Cx36), a gap junction protein found predominantly in inhibitory interneurons throughout the brain, is required for electrical synapses to form between IINs in the brain (Deans et al., 2001; Hormuzdi et al., 2001). Therefore, deletion of Cx36 offers a way to test the role of IIN networks in producing low frequency correlation patterns in the blood oxygen signal.

Mice with Cx36 gene deletion (Cx36−/−) have normal brain anatomy, growth, and fertility (Deans et al., 2001; Hormuzdi et al., 2001). Neural activity, however, is altered in Cx36−/− brains. In brain slices from wild-type (Cx36+/+) mice, chemically inducing IIN activity produced correlated inhibitory post-synaptic potentials (IPSP) between neurons up to 400 μm apart (Deans et al., 2001). In comparison, IPSP correlation is dramatically reduced with Cx36 gene deletion, demonstrating an essential role for Cx36 gap junctions in spatiotemporal coordination of inhibitory activity (Deans et al., 2001). In addition, Cx36 gene deletion resulted in decreased gamma (30–80 Hz) oscillation power *in situ* (Buhl et al., 2003); pharmacologic blockade, as well as genetic deletion of Cx36, caused decreased theta (3–12 Hz) oscillation power in cortical local field potentials *in vivo* (Bissiere et al., 2011; Postma et al., 2011). Thus, Cx36 has a well-defined role in coordinating neural activity within small brain volumes. However, the role of Cx36 and IINs in regulating activity across distant brain regions has not been examined. Previous work has demonstrated coupling between high and low frequency neural oscillations (He et al., 2010), and we are interested in the whole-cortex infra-slow correlates of the high frequency changes seen in Cx36−/− mice.

We hypothesized that IIN networks may influence spontaneous brain activity patterns across large cortical distances. More specifically, we speculated that electrically coupled IIN networks modulate whole-brain spontaneous ISA correlation patterns (or functional connectivity). To test this hypothesis, we performed wide-field optical intrinsic signal (OIS) imaging in Cx36+/+ and Cx36−/− mice to examine whole-cortex spontaneous ISA correlation organization. We found that Cx36 gene deletion resulted in enhanced inter-hemispheric ISA correlation and intra-hemispheric ISA anti-correlation between specific cortical regions. This suggests that electrically coupled IIN networks play a role in limiting ISA synchrony over large cortical distances.

2. Materials & methods

2.1. Mice

All procedures described below were approved by the Washington University Animal Studies Committee in compliance with AAALAC guidelines. Littermate (male and female) Cx36+/+ and Cx36−/− mice on a pure C57Bl6/J background (RRID:MGI:3810169)(Hormuzdi et al., 2001) were raised in standard cages in a dedicated mouse facility with a 12-12 light/dark cycle. All imaging was performed on P90 mice. In total, 19 Cx36+/+ (11 male, 8 female) and 13 Cx36−/− (5 male, 8 female) mice were used in this study.

2.2. Imaging animal preparation

In accord with our previously published animal preparation protocol for fOIS imaging (White et al., 2011), anesthesia was initiated via intraperitoneal injection with a bolus of ketamine-xylazine (1x dose: 86.9 mg/kg ketamine, 13.4 mg/kg xylazine) and animals were allowed 15 min for anesthetic transition. After induction, the animal was placed on a heating pad maintained at 37 °C via feedback from a rectal probe (mTCII, Cell Microcontrols) and its head was secured in a stereotactic frame. The head was shaved and cleaned, a midline incision was made along the top of the head to reflect the scalp and the skull was kept intact.

2.3. Image acquisition

Sequential illumination was provided at four wavelengths by a ring of light emitting diodes (LEDs) placed approximately 10 cm above the mouse's head. The field of view included most of the cerebral cortex (approximately 1 cm^2). Diffuse reflected light was detected by a cooled, frame-transfer EMCCD camera (iXon 897, Andor Technologies); the LED ring and the camera were time-synchronized and controlled via computer using custom written software (MATLAB, Mathworks) at a full frame rate of 30 Hz.

2.4. Image processing

Data from all mice were subjected to an initial quality check prior to spectroscopic analysis. Data runs (5 min) in which reflected light level intensity (mean value over the brain) varied as a function of time by greater than 1% for any wavelength were excluded from further analysis. This preliminary quality control yielded 10–30 min of data per mouse. For subsequent analysis, image light intensity at each wavelength was interpreted using the Modified Beer-Lambert Law, usually expressed as: $\Phi(\mathbf{r},t) = \Phi_0 * \exp(-\Delta\mu_a(\mathbf{r},t) * L)$. Here, $\Phi(\mathbf{r},t)$ is the measured light intensity, Φ_0 is the baseline light intensity, $\Delta\mu_a(\mathbf{r}, t)$ is the change in absorption coefficient due to hemodynamic changes, and L is the optical path length factor for photons in the tissue (Arridge et al., 1992). As there is no pre-stimulus baseline in resting-state experimentation, we normalized relative to the average light intensity at each pixel, resulting in differential measures of absorption at each wavelength at each pixel: $\Delta\mu_{a,\lambda}(\mathbf{r},t) = -\ln(\Phi_\lambda(\mathbf{r},t)/\langle \Phi_{0\lambda}(\mathbf{r},t)\rangle)/L_\lambda$. Absorption coefficient data were converted to hemoglobin (Hb) concentration changes by inverting the system of equations, $\Delta\mu_{a,\lambda}(\mathbf{r},t) = E_{\lambda,i}\,\Delta[Hb_i](\mathbf{r},t)$ (where E is the extinction coefficient matrix, and *i* runs over hemoglobin species). This inversion was performed using least-squares methods, yielding changes in oxygenated hemoglobin (HbO) and deoxygenated hemoglobin (HbR) at each pixel at each time point. We calculated total hemoglobin (HbO + HbR) for all analyses used in this study. Differential changes in hemoglobin concentration were filtered to retain the infra-slow activity/-functional connectivity band (0.01–0.1 Hz) following previous human functional connectivity algorithms (Fox et al., 2005). After filtering, each pixel's time series was downsampled from 30 Hz to 1 Hz, and all further analysis was performed only on those pixels labeled as brain using a manually constructed brain mask. The time traces of all pixels defined as brain were averaged to create a global brain signal. This global signal was regressed from every pixel's time trace to remove global sources of variance; global signal regression was applied independently on each contiguous imaging session.

2.5. Image co-registration

Image sequences for each mouse (as well as the brain mask for each mouse) were affine-transformed to a common atlas space determined by the positions of the junction between the coronal suture and sagittal suture (posterior to the olfactory bulb and cerebrum along midline) and lambda, as previously reported (Bauer et al., 2014). Bregma was not visible in all mice, and was calculated based on the above two anatomical landmarks. The anterior-posterior stretch was set equal to the medial-lateral stretch, and all transformed images were centered at bregma. A common brain mask shared by all mice and used in every analysis in this study was calculated and made symmetric by reflection across the midline.

2.6. ISA correlation (functional connectivity) analysis

Pearson correlation was calculated for each pixel pair's time series of total hemoglobin data. Correlation difference PCA segmentation was performed by applying spatial principal components analysis to the whole-cortex correlation difference matrix calculated from the difference in average correlation at each pixel between the two groups.

2.7. Data-driven region of interest generation

To generate ROIs, 3 Cx36+/+ and 3 Cx36−/− mice were randomly selected. The Δcorrelation matrix (Fig. S1C) was generated by subtracting the Cx36−/− correlation matrix (the matrix of every pixel-pixel correlation value; Fig. S1B) from the Cx36+/+ correlation matrix (Fig. S1A), resulting in a matrix that identifies pixel pairs with the greatest ISA correlation differences between Cx36+/+ and Cx36−/− mice. Principal component analysis of the Δcorrelation matrix was used to generate a Δcorrelation PC map that demonstrated focal territories of correlation increases and decreases (Fig. 1F). Prior work showing robust interhemispheric spontaneous correlation symmetry (Bero et al., 2012; Kraft et al., 2017; White et al., 2011) argued that inter-hemispheric asymmetry was due to noise from low mouse number. Thus, we averaged each homotopic pixel. This process formed 2 distinct ROIs on each hemisphere that were thresholded at 60% of the maximum magnitude over the entire Δcorrelation PC map. We excluded the 3 most medial pixels on the left and right anterior ROI closest to the midline in order to better separate the ROIs in each hemisphere. We also excluded the small number of pixels over the anterior sinus that did not correspond to a functional region (Fig. 1G).

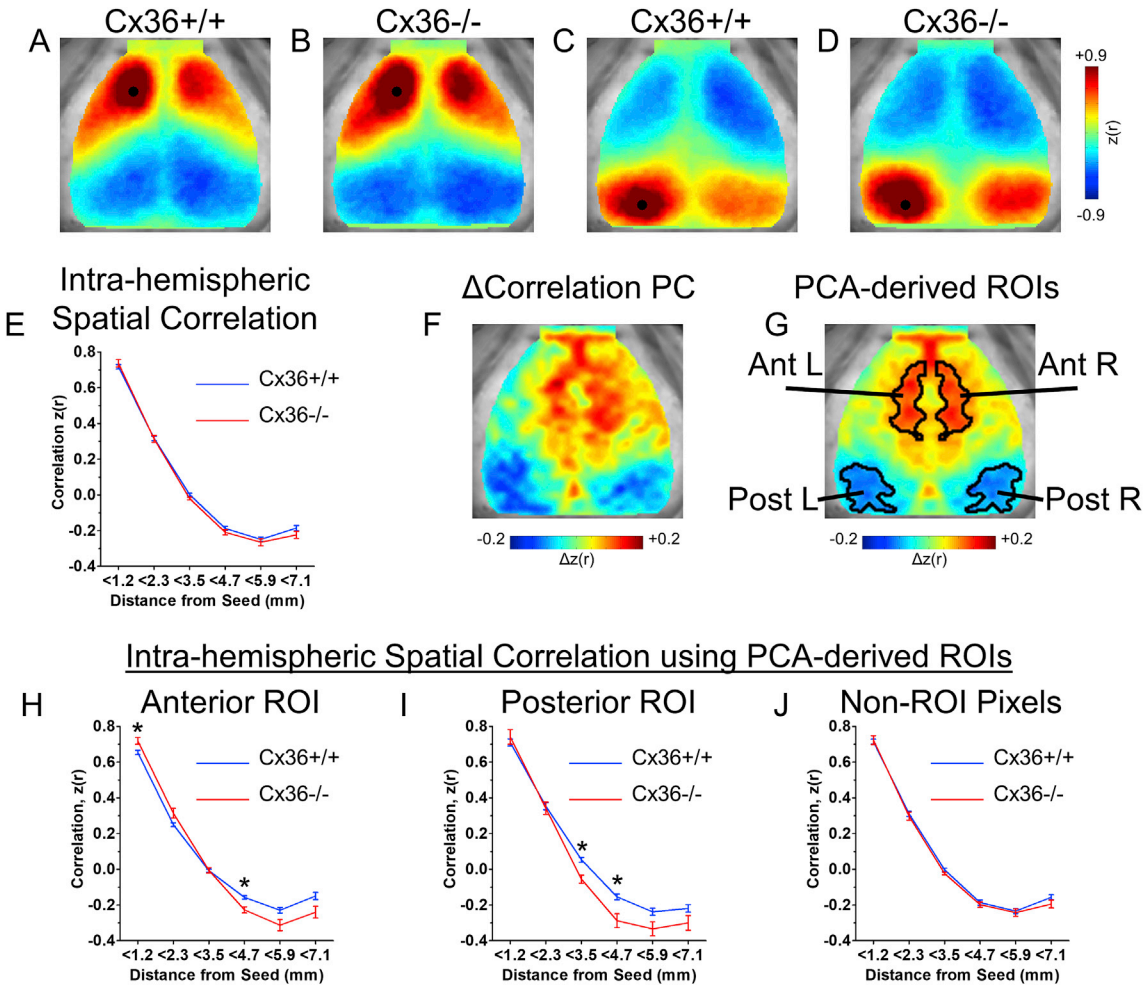

Fig. 1. Cx36 deletion altered spatial ISA correlation relationships in specific cortical regions. **(A–D)** Group averaged seeded correlation maps for **(A,B)** an anterior seed and **(C,D)** a posterior seed. Consistent with previous studies, all maps showed high correlation surrounding the seed, high homotopic correlation, and anterior-posterior anti-correlation. Qualitatively, the Cx36−/− mice have increased correlation values near the seed. **(E)** Group averaged correlation values vs. distance for every intra-hemispheric pixel. For each mouse, the correlation vs. distance curve from the left and right hemisphere was averaged before group averaging was performed. Using a subset of mice (Cx36+/+ n = 3, Cx36−/− n = 3), PCA was performed on the correlation differences between groups in order to find ROIs that may be selectively influenced by Cx36. **(F)** The first principal component derived from Δcorrelation PCA reveals distinct anterior and posterior ROIs with ISA correlation patterns that differ between Cx36+/+ and Cx36−/− groups. **(G)** Anterior and Posterior ROIs defined after smoothing, bilateral averaging, and thresholding of the Δcorrelation PC in (F). These ROIs were used for analysis on an independent set of mice (Cx36+/+ n = 16, Cx36−/− n = 10). **(H–J)** Spatial correlation values for pixels within the ROIs from (G). **(H)** Within the anterior ROI, Cx36 deletion caused increased correlation for nearby pixel pairs (<1.2 mm), and increased anti-correlation for more distant pixel pairs (3.5mm–4.7 mm). **(I)** Within the posterior ROI, Cx36 deletion resulted in increased anti-correlation at further distances (3.5mm–4.7 mm). The correlation vs. distance curve was calculated between all pixels within the ROIs and every other pixel in the same hemisphere. **(J)** Correlation vs. distance relationship for pixels outside of the ROIs from (G). No differences were found for pixels in this area. *P < 0.0083 (0.05/number of distance bins; determined using Student's *t*-test with Bonferonni correction).

2.8. Correlation gradient maps

Gradient maps in Fig. 4 were created by first computing the 2-dimensional spatial derivative for each pixel-seeded correlation map in the cortical field of view, and then averaging the spatial derivatives over pixels. We implemented the spatial derivative computation using the imgradient function in MATLAB (Mathworks) with the Sobel gradient operator. For these calculations, values cannot be calculated for pixels on the edge of the image. As a result, the displayed gradient maps are smaller compared to the correlation maps due to loss of the edge pixel.

2.9. Statistics

All single-dimension statistical comparisons were assessed with Student's *t*-test. The statistical threshold was set at 0.05 divided by the number of comparisons performed. Statistical significance of correlation differences in spatial maps (Fig. 3I-L) was assessed on a cluster-wise basis using threshold-extent criteria computed by extensive permutation resampling (Hacker et al., 2012; Hayasaka and Nichols, 2003; Kraft et al., 2017).

3. Results

3.1. Cx36 gene deletion altered spatial ISA correlation in specific cortical regions

We first examined whether IIN gap junctions modulate local correlation in ISA. Given previous work showing Cx36 deletion reduces inhibitory tone synchrony over short distances (up to 400 μm) (Deans et al., 2001), we hypothesized that ISA correlation may be most dramatically influenced over short distances in Cx36−/− mice.

ISA correlation relationships can be visualized by choosing seed pixels on the cortex and examining the correlation in spontaneous ISA between that seed and every other pixel on the cortex (Fig. 1A–D). To provide a qualitative description of ISA correlation maps, we arbitrarily chose an anterior seed (Fig. 1A,B) and a posterior seed (Fig. 1C and D) in the group-averaged ISA correlation data from Cx36+/+ (Fig. 1A,C) and Cx36−/− (Fig. 1B,D) mice. These ISA correlation maps revealed the basic tenets of cortical ISA correlation we have found previously in the mouse: high positive correlation surrounding the seed, high inter-hemispheric homotopic correlation, and anti-correlation between the anterior and posterior regions within the same hemisphere (Bauer et al., 2014; Kraft et al., 2017; White et al., 2011).

Qualitative inspection of the correlation maps in Fig. 1A–D suggests Cx36 gene deletion resulted in increased positive correlation magnitude in the pixels surrounding the seed as well as an increased anterior/posterior anti-correlation magnitude (henceforth, we refer to correlation magnitude without explicitly stating "magnitude"). However, these seeds are only 2 pixels of the cortical space. To quantify if electrically coupled IIN networks influence ISA correlation in a distance-dependent manner for the entire cortical space, we explored the relationship between distance and correlation for all intra-hemispheric pixel pairs. We accomplished this by first examining the spatial correlation curve of each pixel: each intra-hemispheric pixel-pixel pair's correlation value and separation distance was calculated, and the average correlation vs. distance curve was generated (Fig. 1E). In Cx36+/+ mice this relationship shows high positive correlation values at short distances, decreasing correlation with distance, and anti-correlation occurs at longer distances. Cx36 gene deletion did not alter this relationship (Fig. 1E).

We suspected there might be spatially specific correlation relationships that are selectively influenced by Cx36. Previous work has shown that Cx36 has a non-uniform distribution throughout the cortex (Deans et al., 2001; Shigematsu et al., 2019), and it is not currently known whether distinct IIN networks exist within the brain. Thus, we next tested whether Cx36 has a non-uniform influence on correlation relationships. We used a non-biased, data-driven approach to identify regions of interest (ROIs) with selective differences in spontaneous correlation between Cx36+/+ and Cx36−/− mice. A subset of randomly selected Cx36+/+ and Cx36−/− mice were used to identify ROIs, and these ROIs were used for analysis in independent mice.

Using the random subset of Cx36+/+ and Cx36−/− mice (Cx36+/+ n = 3, Cx36−/− n = 3), we performed principal component analysis on the Δcorrelation matrix (Fig. S1). The Δcorrelation matrix (Fig. S1C) was generated by subtracting the Cx36−/− correlation matrix (the matrix of every pixel-pixel correlation value; Fig. S1B) from the Cx36+/+ correlation matrix (Fig. S1A), resulting in a matrix that identifies pixel pairs with the greatest ISA correlation differences between Cx36+/+ and Cx36−/− mice. Principal component analysis of the Δcorrelation matrix revealed that the first principal component (PC) explained 28% of the variance (Fig. S1F). Projection of the Δcorrelation matrix on the corresponding eigenvector generated a Δcorrelation PC map that demonstrated focal territories of correlation increases and decreases (Fig. 1F). These areas were used to define the ROIs that were used for subsequent analysis performed on a separate, independent set of mice (Fig. 1G).

Using a set of separate Cx36+/+ and Cx36−/− (Cx36+/+ n = 16, Cx36−/− n = 10), we looked at the relationship between intra-hemispheric distance and correlation for pixels within the experimentally generated ROIs from Fig. 1G. Correlation between the anterior ROI pixels and all other pixels within the same hemisphere showed increased anti-correlation at longer distances and increased correlation at shorter distances in Cx36−/− mice (Fig. 1H). Correlation between the posterior ROI pixels and all other intra-hemispheric pixels showed increased anti-correlation at longer distances in Cx36−/− mice compared to Cx36+/+ mice (Fig. 1I). For pixels outside of these ROIs, there was no difference in the spatial correlation relationship (Fig. 1J). Thus, Cx36 deletion enhanced intra-hemispheric correlation and anti-correlation for selective cortical regions.

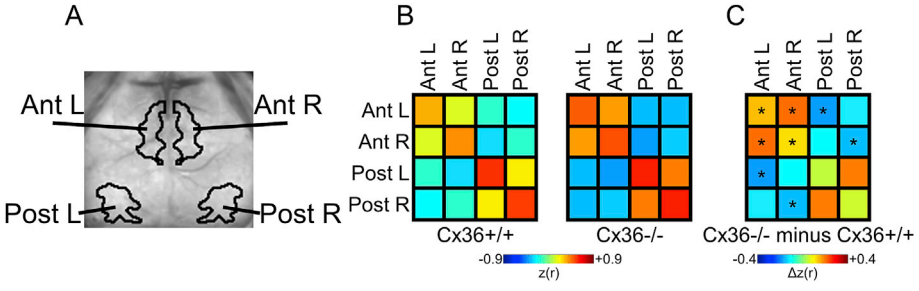

Fig. 2. Cx36 deletion increased inter-hemispheric correlation and intra-hemispheric anti-correlation between specific ROIs. **(A)** ROIs used for analysis. **(B)** Average correlation values for all pixels within and between all ROIs in Cx36+/+ and Cx36−/− mice. **(C)** Cx36−/− minus Cx36+/+ Δcorrelation matrix with statistically significant correlations marked. For the Ant. ROIs, local and homotopic correlation was increased in Cx36−/− mice. In addition, the intra-hemispheric Ant.-Post. anti-correlation was increased in Cx36−/− mice. Post. ROI homotopic correlation was increased in Cx36−/− mice, but it was not statistically significant. *P < 0.005 (0.05/number of correlations examined; determined using Student's *t*-test with Bonferonni correction). Cx36+/+ n = 16, Cx36−/− n = 10.

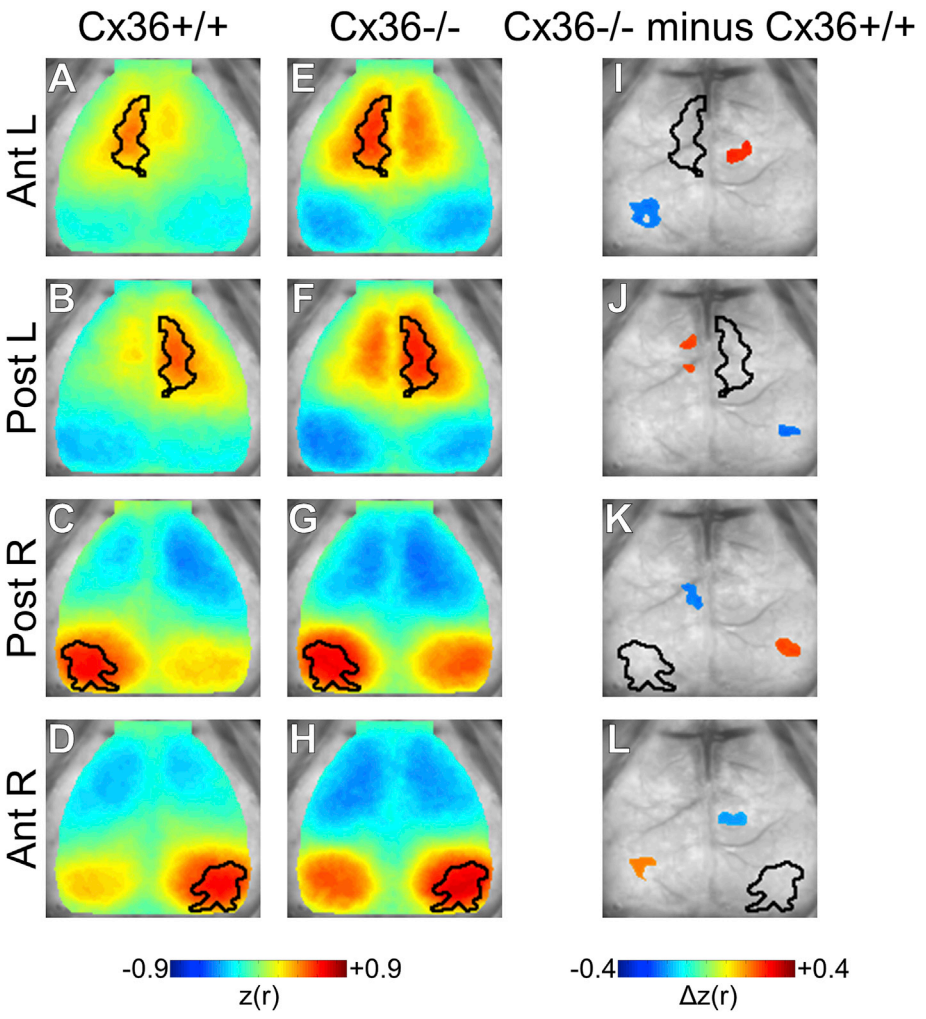

Fig. 3. Spatial distribution of correlation changes with Cx36 deletion. Seeded correlation maps for **(A–D)** Cx36+/+ and **(E–H)** Cx36−/− mice. Seeded regions are outlined in black. Enhanced homotopic correlation and intra-hemispheric anti-correlation were qualitatively apparent in Cx36−/− mice. **(I–L)** Statistically masked correlation difference maps (Cx36−/− minus Cx36+/+) for each ROI. Significance was determined using spatial cluster-wise threshold-extent criteria (see methods). **(I,J)** For Ant. ROIs, Cx36−/− mice demonstrated increased homotopic correlation and increased Ant.-Post. ROI anti-correlation for each hemisphere. Note that the increased local correlation seen qualitatively in E vs. A and F vs. B was not statistically significant. **(K,L)** Post. ROIs showed regionally selective increases in intra-hemispheric anti-correlation and increased inter-hemispheric correlation. The inter-hemispheric correlation increases were centered outside of the homotopic Post. ROI. Cx36+/+ n = 16, Cx36−/− n = 10.

3.2. Cx36 gene deletion increased inter-hemispheric correlation and anti-correlation in select cortical regions

In order to examine how Cx36 influenced inter-hemispheric correlation relationships we examined both the intra- and inter-hemispheric ISA correlations between our data-driven ROIs (Fig. 2). First we used ROI-sorted matrices showing the mean correlation value for every set of ROI pairs (Fig. 2B). Qualitative inspection of these correlation matrices showed a clear influence of Cx36 on the intra- and inter-hemispheric correlation relationships. Subtracting these two matrices to generate the Δcorrelation matrix for these ROIs showed that, indeed, Cx36−/− mice have increased inter-hemispheric homotopic correlation and increased intra-hemispheric anti-correlation (Fig. 2C). Consistent with Fig. 1, the intra-hemispheric Anterior ROI and Posterior ROIs had increased anti-correlation in the Cx36−/− mice compared to Cx36+/+ mice. Also, the Anterior ROIs had increased local, or within-ROI, correlation. This increased local correlation demonstrates an increased spread of correlation surrounding the seeds within the Anterior ROI within Cx36−/− mice. In addition, this analysis showed that Cx36 deletion increased homotopic correlation between the Anterior ROIs. Homotopic correlation between the Posterior ROIs was increased, but the difference did not reach statistical significance (Fig. 2C). Furthermore, this analysis showed increased anti-correlation between the anterior and posterior regions of separate hemisheres (non-homotopic interhemispheric relationships) in Cx36−/− mice compared to Cx36+/+ mice.

To better appreciate the whole-cortex topography of ISA correlation changes for our data-driven ROIs we calculated the whole-cortex correlation maps seeded by our ROIs (Fig. 3). Using this approach, clear differences were present between Cx36+/+ and Cx36−/− correlation maps (Fig. 3A–H). Consistent with previous analyses, Cx36−/− maps had largely increased homotopic inter-hemispheric correlation and intra-hemispheric anti-correlation for the ROIs examined. In addition, Cx36−/− mice had increased anti-correlation between the anterior and posterior regions of separate hemisheres (non-homotopic interhemispheric relationships) as was seen in the previous analysis. Statistical significance of topographical correlation differences between groups was assessed on a spatial cluster-wise basis using threshold-extent criteria computed by extensive permutation resampling (Hacker et al., 2012; Hayasaka and Nichols, 2003; Kraft et al., 2017).

An additional key finding in the statistically masked difference maps was that both the left and right Posterior ROIs showed contralateral clusters of increased correlation that were just outside of the homotopic ROI (Fig. 3K,L). Thus for the Posterior ROIs, Cx36 deletion increased the spatial spread of positive homotopic correlation. A modest increase of correlation surrounding the Anterior ROI was observed, but this effect was not statistically significant. The inter-hemispheric anti-correlation increases seen in Cx36−/− mice were not statistically significant. Altogether, this analysis was overall consistent with the previous metrics and statistical tests: Cx36 deletion increased ISA correlation and anti-correlation for cortical ROIs separated by long distances within and across hemispheres.

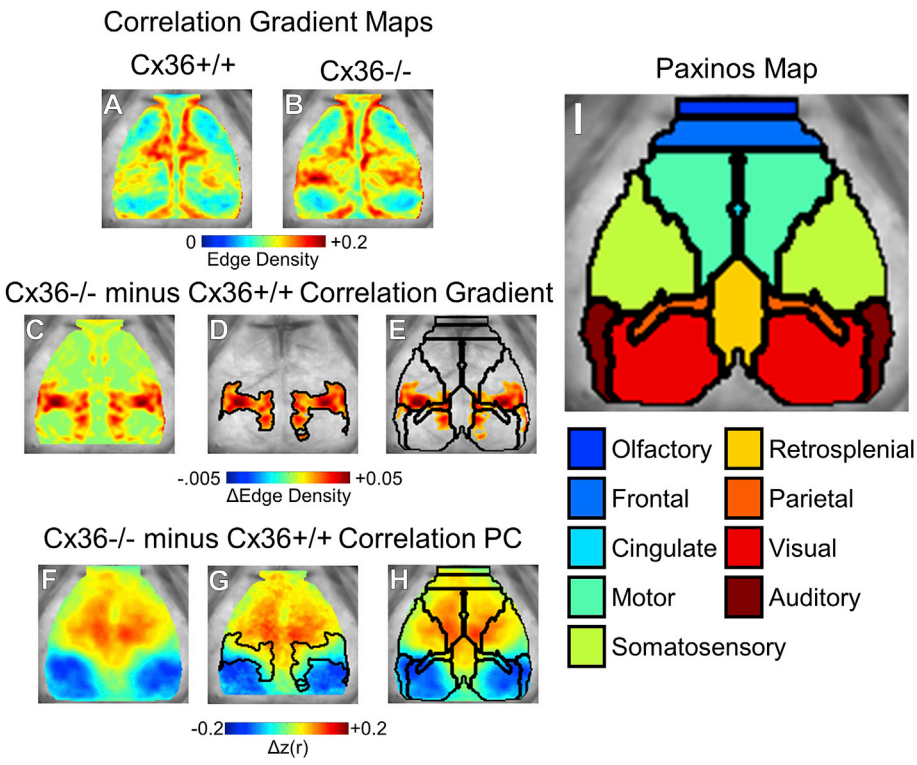

Fig. 4. Cx36 deletion caused a wider anterior-posterior correlation transition gradient. **(A–B)** Correlation gradient maps for **(A)** Cx36+/+ mice and **(B)** Cx36−/− mice. The brain space is smaller compared to Figs. 1–3 because gradient values are not calculated at the edge. **(C)** Cx36−/− minus Cx36+/+ gradient difference map revealed a focally increased correlation transition gradient on the anterior-posterior axis. **(D)** Threshold-masked and outlined gradient differences. **(E)** Thresholded gradient differences shown with overlaid Paxinos anatomy demonstrated that these gradient differences occur at the border of several anatomical regions separated on the anterior-posterior axis. **(F)** The Δcorrelation PC determined from PCA on correlation differences between all mice analyzed. This Δcorrelation PC was similar to the Δcorrelation PC found in a subset of mice in Fig. 1F. Δcorrelation PC with overlaid **(G)** correlation gradient differences and **(H,I)** Paxinos anatomical boundaries and atlas for reference. Cx36+/+ n = 19, Cx36−/− n = 13.

3.3. Cx36 gene deletion altered the sharp transition between functionally distinct brain regions

The cortex can be partitioned into distinct regions based on sharp transitions in resting state correlation patterns that occur across functionally distinct ROIs. Resting state correlation patterns are markedly homogenous within a single functional region, but dramatic transition occurs at the border between separate regions. As a result, the brain contains discrete territories of high ISA correlation pattern similarity that are separated by narrow edges of transition. Previous work has shown that human functional borders generated using sharp correlation pattern transitions were well aligned with architectonic mapping suggesting anatomical relevance of these functional borders (Gordon et al., 2016).

Given the previous results showing IIN networks modulate synchrony across long distances, we wondered how electrically coupled IIN networks might influence functional transitions between regions. Using all imaged Cx36+/+ and Cx36−/− mice (Cx36+/+ n = 19, Cx36−/− n = 13), we generated correlation edge gradient maps (Fig. 4A and B). In Cx36+/+ mice, an anterior-posterior gradient border zone was apparent but narrow, suggesting abrupt correlation changes occur over the anterior-posterior correlation transition (Fig. 4A). Cx36−/− gradient maps showed increased spatial derivative values (edge density) that separated the anterior and posterior cortex over a wider distance (Fig. 4B). This suggests Cx36 deletion resulted in a widening of the sharp gradient border zone between the anterior and posterior hemi-cortices. Subtracting the two, it is clear that Cx36+/+ mice had much narrower correlation transition gradient border zones along the anterior-posterior axis (Fig. 4C). This suggests Cx36 is required for the normal sharp functional transitions seen in wildtype mice between the anterior and posterior cortical regions.

Using the entire set of mice (including the mice used for ROI generation in previous sections), we performed PCA on the Cx36+/+ vs. Cx36−/− Δcorrelation matrix to generate the Δcorrelation PC map (Fig. 4F). This Δcorrelation PC explained 39% of the variance (Fig. S2) and was similar to the Δcorrelation PC map generated from the subset of mice in Fig. 1F. Overlaying the transition gradient changes on the Δcorrelation PC map demonstrated that Cx36 deletion resulted in a widened transition zone between the anterior and posterior regions (Fig. 4G). Comparing this transition gradient change map to the Paxinos mouse brain atlas (Fig. 4H), it was apparent that the borders overlap between the two maps, suggesting that the gradient maps are delineating anatomical territories. Thus in addition to altering spontaneous activity correlation, Cx36 deletion "blurs" the anterior-posterior transition from one anatomical region to another. This suggests that electrically coupled IIN networks play a role in creating sharp transitions between functionally defined regions.

4. Discussion

In this study we used wide-field OIS imaging in mice deficient for Cx36, the gap junction protein that forms electrical synapses between IINs, to examine the role of IIN electrical synapses in shaping spontaneous activity correlation patterns over the entire cerebral cortex. We found that disrupting Cx36-mediated electrical coupling in IIN networks resulted in increased ISA correlation and anti-correlation between distant cortical regions both within and across hemispheres.

4.1. Cx36 influence on intra-hemispheric correlation organization

Anti-correlations in spontaneous brain activity led to some of the earliest descriptions of spontaneous activity network organization (Fox et al., 2005; Greicius et al., 2003). Spontaneous anti-correlations separate areas that have respective increases and decreases in activity during focused tasks (Cabeza and Nyberg, 2000; Corbetta and Shulman, 2002; Fox et al., 2005; Greicius et al., 2003; McKiernan et al., 2003; J. R. Simpson et al., 2000; Simpson et al., 2001). One of the most salient examples of anti-correlated activity is seen in the relationship between the dorsal attention network and default mode network in humans (Fox et al., 2005). Activity in the default mode network decreases during attention demanding tasks, and is thought to be driven by the brain pivoting from self-referential activity to task-directed activity requiring focused attention (Fox et al., 2005; Gusnard et al., 2001; Raichle et al.,

2001). Importantly, global signal regression, a pre-processing step used in this study, zero-means correlation data and results in the spontaneous correlation histogram being shifted from mostly positive to balanced positive and negative values (for review see (Murphy and Fox, 2017)). Thus, the anti-correlated spontaneous activity seen after global signal regression represents brain networks with system-specific activity profiles regardless of the exact magnitude of their correlation. In addition, global signal regression reduces non-neural sources of noise such as respiration and movement (Birn, 2012; Power et al., 2014; Yan et al., 2013), and delineates functionally connected networks in a manner that better correspond to brain anatomy (Fox et al., 2009). Importantly, seeded Pearson correlation maps from our data with GSR and without GSR both showed that Cx36 gene deletion results in decreased correlation between the anterior and posterior regions, as well as increased homotopic correlation (Fig. S3).

Our results demonstrate that electrically coupled IIN networks play a role in limiting anti-correlations. Spontaneous anti-correlations are believed to be important in segregating distinct processing streams, but electrically coupled IIN networks may limit anti-correlation to optimally balance integration and segregation across separate networks.

Moreover, the correlation transition gradients in Cx36−/− mice were broader than those in Cx36+/+ mice. While increased anti-correlation magnitude can logically produce a widened transition gradient, they do not necessitate one. The transition zone is determined by the spatial efficiency over which correlation structure changes from one pattern to another. Our results suggest that Cx36 plays a role in establishing an abrupt transition between separate cortical regions. We speculate that synchronized inhibition is critical to maintain sharp transitions, and sharp transitions may be important to optimize network function. Previous work has shown that Cx36−/− mice have impaired performance in complex, multi-domain tasks including sensorimotor learning, complex spatial learning, and object recognition (Frisch et al., 2005). The disrupted functional transitions we show in Cx36−/− mice may be a network-level correlate of impaired multi-domain behavioral performance.

4.2. Cx36 influence on inter-hemispheric correlation organization

In addition to the intra-hemispheric anti-correlation enhancement in Cx36−/− mice, we also found increased inter-hemispheric correlation between the left and right Anterior ROIs as well as the left and right Posterior ROIs (for the homotopic relationships, roughly speaking). Homotopic correlations are especially robust in humans and they are present in all species that have been examined (Biswal et al., 1995; Chan et al., 2015; Fox et al., 2005; Pawela et al., 2008; Power et al., 2011; Stafford et al., 2014; Vincent et al., 2007; White et al., 2011). Indeed, this phenomenon extends to the mouse and has been observed using fMRI, fOIS, genetically encoded calcium imaging, genetically encoded glutamate imaging, and voltage sensitive dyes (Chan et al., 2015; Ma et al., 2016; Matsui et al., 2016; Stafford et al., 2014; White et al., 2011; Wright et al., 2017; Xie et al., 2016).

Our results suggest that electrically coupled IIN networks play a role in restricting spontaneous synchrony between homotopic cortical regions. This is especially interesting given that homotopic correlation decrement is a powerful biomarker of neurologic disease (Carter et al., 2010; Chase, 2014). Cx36 deletion, on the other hand, increased certain homotopic correlations in our study, but previously published work has shown Cx36 deletion caused deficits in complex motor learning and experience-dependent plasticity (Bissiere et al., 2011; Frisch et al., 2005; Postma et al., 2011; Wang and Belousov, 2011; Zlomuzica et al., 2012). Recently, we showed that binocular visual deprivation during visual critical periods in mice causes increased homotopic correlation between visual cortices (Kraft et al., 2017). Altogether, it is clear homotopic correlation is fine-tuned to a specific level by normal developmental processes, and increased homotopic connectivity can be associated with abnormal states.

By limiting inter-hemispheric correlation, each cortical hemisphere may be able to operate with more independence. Ideal brain function must involve a balance between system independence and integration (Sporns, 2013; Tononi et al., 1994). Over-synchronization across all systems may limit the ability of each brain system to handle specific tasks independently. On the other hand, complete asynchrony may prevent the cross-system communication required for high order integration. Thus through the observed effect on ISA decoupling, electrical coupled IIN networks may enable better parallel processing for handling complex scenarios.

4.3. Anatomy of electrically coupled IIN networks and spontaneous ISA correlation organization

The spatial distribution of cortical Cx36 expression and electrically coupled IIN networks is not well defined and this makes interpreting our data a challenge. Cx36 expression is likely driven by developmental processes that enable the formation of electrically-coupled inhibitory networks to support ideal brain function. However, the exact mechanism by which electrical gap junctions influence both local and long-distance cortical connections remains unknown. Within the rodent barrel cortex, within-barrel IINs form gap junctions exclusively with extra-barrel septal IINs. These extra-barrel IINs form widespread electrical connections both within their home cortical column and across multiple outside cortical columns (Shigematsu et al., 2019). The neurophysiological implications of this architecture are not known, but this micro-anatomy may allow electrically-coupled IIN networks to play a role in integrating cortical information across multiple cortical columns.

By enabling bidirectional electrical coupling between multiple IINs over a larger scale, Cx36 gap junctions could allow electrical inhibitory signal integration over any brain volume. By coordinating inhibitory activity on a larger scale, IINs may play an important role in modulating functional territories. Future work to delineate individual IIN networks over larger cortical volumes will be required in order to better understand how their topographically selective effects are achieved. Nonetheless the best current data suggests the reach of electrically coupled IINs is rather limited. In wild-type mice, IPSP demonstrate marked temporary synchrony over a range of 400 μm. Cx36 gene deletion attenuates IPSP correlation over this distance demonstrating a critical role of gap junctions in coordinating inhibitory tone. (Deans et al., 2001). Given this limit, it is unclear how disrupting electrically coupled IIN networks influenced spontaneous ISA correlation relationships across different functional regions spanning over 5 mm.

It is thought that electrically coupled IIN networks may be coordinated by longer-distance axonal inputs. Long-distance axonal connections are thought to be critical for proper coordination of coherent signals (Felleman and Van Essen, 1991; Jinno et al., 2007). In the case of homotopic cortical relationships, it has been suggested that transcallosal projections have both excitatory and inhibitory interhemispheric influences (Bloom and Hynd, 2005). Transcallosal projections may synapse on IINs (directly or indirectly) and exert coordinated interhemispheric inhibition that is carefully balanced with excitatory signaling to generate a precise excitatory/inhibitory balance. Electrical coupling amongst these IINs may be crucial for proper inhibition across hemispheres. Likewise, long-distance intra-hemispheric connections may be important for limiting out of phase synchrony that produces anti-correlated activity. Both glutamatergic and GABAergic long-range axons connecting different cortical areas have been demonstrated (Jinno et al., 2007; Somogyi et al., 1998). Excitatory neurons could link to IIN networks and modulate their inhibitory tone. In addition, the existence of long-range GABAergic synapses makes it possible that IIN networks may be able to form long distance inhibitory projections coordinate inhibition over long ranges. Future work will need to examine this possibility.

4.4. Limitations

All fOIS experiments performed in this study were done under ketamine/xylazine anesthesia. Recent work in mice has shown that zero-lag cortical correlations in slow activity are stable across wake and ketamine/xylazine anesthesia states (Silasi et al., 2016). This is in agreement with data showing stability of low frequency correlation across states of consciousness in humans (Picchioni et al., 2013).

Important potential confounds that can occur when using knock-out mice must be considered. Cx36 gene deletion may result in compensatory neurodevelopment. Furthermore, Cx36 may play an unknown-role in hemodynamics that could influence physiology relevant to neuroimaging.

Previous work using Cx36−/− brain slices *in vitro* and awake Cx36−/− mice *in vivo* have demonstrated decreased gamma power with Cx36 deletion. However, *in vivo* work has revealed that some differences in Cx36−/− mice are accentuated under specific conditions. More specifically gamma power differences between Cx36+/+ and Cx36−/− mice were larger during wheel running than during sleep (Buhl et al., 2003), and theta power increases following plasticity paradigms were absent in Cx36−/− mice (Bissiere et al., 2011; Postma et al., 2011). Thus, the resting state differences we see may not be capturing more robust network-level effects that occur during complex tasks or after learning. Future work will be required to further understand state-dependent effects.

Data and code availability statement

Data and code is available upon direct request to the corresponding author.

Author contributions

AWK and JML designed experiments. AWK and ZPR collected data. AM and AWK processed and analyzed data. AWK, AM, ZPR, and JML wrote the manuscript with help from all co-authors. All authors read and approved the final manuscript. JML supervised all aspects of the project.

CRediT authorship contribution statement

Andrew W. Kraft: Conceptualization, Methodology, Software, Validation, Formal analysis, Investigation, Writing - original draft, Writing - review & editing, Visualization. **Anish Mitra:** Methodology, Software, Formal analysis, Writing - original draft, Writing - review & editing, Visualization. **Zachary P. Rosenthal:** Methodology, Investigation, Writing - original draft, Writing - review & editing, Visualization. **Nico U.F. Dosenbach:** Conceptualization, Writing - original draft. **Adam Q. Bauer:** Conceptualization, Software, Visualization, Methodology. **Abraham Z. Snyder:** Conceptualization, Writing - review & editing. **Marcus E. Raichle:** Resources, Funding acquisition. **Joseph P. Culver:** Resources, Funding acquisition. **Jin-Moo Lee:** Conceptualization, Resources, Project administration, Funding acquisition, Writing - original draft, Writing - review & editing.

Acknowledgements

This work was supported in part by National Institutes of Health grants R01NS084028 (J.-M.L.), R37NS110699 (J.-M.L.), R01NS094692 (J.-M.L.), F31NS089135 (A.W.K), R01NS078223 (J.P.C.), P01NS080675 (J.P.C.), P30NS048056 (A.Z.S.), NS080675 (M.E.R. and A.Z.S.), R01NS102870 (AQB), K25NS083754 (A.Q.B), F30MH106253 (A.M.) and American Heart Association grants 13POST14240023 (A.Q.B) and 14PRE18410013 (A.W.K). Cx36 ± mice were a generous gift from Gary L. Westbrook, M.D. (Vollum Institute, Oregon Health & Science University, Portland, OR).

Appendix A. Supplementary data

Supplementary data to this article can be found online at https://doi.org/10.1016/j.neuroimage.2020.116810.

References

Allen, G., et al., 2007. Reduced hippocampal functional connectivity in Alzheimer disease. Arch. Neurol. 64 (10), 1482–1487.
Arridge, S.R., Cope, M., Delpy, D.T., 1992. The theoretical basis for the determination of optical pathlengths in tissue: temporal and frequency analysis. Phys. Med. Biol. 37 (7), 1531–1560.
Bauer, A.Q., et al., 2014. Optical imaging of disrupted functional connectivity following ischemic stroke in mice. Neuroimage 99, 388–401.
Bero, A.W., et al., 2012. Bidirectional relationship between functional connectivity and amyloid-beta deposition in mouse brain. J. Neurosci. 32 (13), 4334–4340.
Birn, R.M., 2012. The role of physiological noise in resting-state functional connectivity. Neuroimage 62 (2), 864–870.
Bissiere, S., et al., 2011. Electrical synapses control hippocampal contributions to fear learning and memory. Science 331 (6013), 87–91.
Biswal, B., et al., 1995. Functional connectivity in the motor cortex of resting human brain using echo-planar MRI. Magn. Reson. Med. 34 (4), 537–541.
Bloom, J.S., Hynd, G.W., 2005. The role of the corpus callosum in interhemispheric transfer of information: excitation or inhibition? Neuropsychol. Rev. 15 (2), 59–71.
Buhl, D.L., et al., 2003. Selective impairment of hippocampal gamma oscillations in connexin-36 knock-out mouse in vivo. J. Neurosci. 23 (3), 1013–1018.
Buzsaki, G., Chrobak, J.J., 1995. Temporal structure in spatially organized neuronal ensembles: a role for interneuronal networks. Curr. Opin. Neurobiol. 5 (4), 504–510.
Cabeza, R., Nyberg, L., 2000. Imaging cognition II: an empirical review of 275 PET and fMRI studies. J. Cognit. Neurosci. 12 (1), 1–47.
Carter, A.R., et al., 2010. Resting interhemispheric functional magnetic resonance imaging connectivity predicts performance after stroke. Ann. Neurol. 67 (3), 365–375.
Chan, A.W., et al., 2015. Mesoscale infraslow spontaneous membrane potential fluctuations recapitulate high-frequency activity cortical motifs. Nat. Commun. 6, 7738.
Chase, A., 2014. Alzheimer disease: altered functional connectivity in preclinical dementia. Nat. Rev. Neurol. 10 (11), 609.
Corbetta, M., Shulman, G.L., 2002. Control of goal-directed and stimulus-driven attention in the brain. Nat. Rev. Neurosci. 3 (3), 201–215.
Deans, M.R., et al., 2001. Synchronous activity of inhibitory networks in neocortex requires electrical synapses containing connexin36. Neuron 31 (3), 477–485.
Evans, W.H., Martin, P.E., 2002. Gap junctions: structure and function (Review). Mol. Membr. Biol. 19 (2), 121–136.
Felleman, D.J., Van Essen, D.C., 1991. Distributed hierarchical processing in the primate cerebral cortex. Cerebr. Cortex 1 (1), 1–47.
Fox, M.D., Raichle, M.E., 2007. Spontaneous fluctuations in brain activity observed with functional magnetic resonance imaging. Nat. Rev. Neurosci. 8 (9), 700–711.
Fox, M.D., et al., 2009. The global signal and observed anticorrelated resting state brain networks. J. Neurophysiol. 101 (6), 3270–3283.
Fox, M.D., et al., 2005. The human brain is intrinsically organized into dynamic, anticorrelated functional networks. Proc. Natl. Acad. Sci. U. S. A. 102 (27), 9673–9678.
Frisch, C., et al., 2005. Stimulus complexity dependent memory impairment and changes in motor performance after deletion of the neuronal gap junction protein connexin36 in mice. Behav. Brain Res. 157 (1), 177–185.
Galarreta, M., Hestrin, S., 2002. Electrical and chemical synapses among parvalbumin fast-spiking GABAergic interneurons in adult mouse neocortex. Proc. Natl. Acad. Sci. U. S. A. 99 (19), 12438–12443.
Gordon, E.M., et al., 2016. Generation and evaluation of a cortical area parcellation from resting-state correlations. Cerebr. Cortex 26 (1), 288–303.
Grayson, D.S., et al., 2016. The rhesus monkey connectome predicts disrupted functional networks resulting from pharmacogenetic inactivation of the amygdala. Neuron 91 (2), 453–466.
Greicius, M.D., et al., 2003. Functional connectivity in the resting brain: a network analysis of the default mode hypothesis. Proc. Natl. Acad. Sci. U. S. A. 100 (1), 253–258.
Gusnard, D.A., Raichle, M.E., Raichle, M.E., 2001. Searching for a baseline: functional imaging and the resting human brain. Nat. Rev. Neurosci. 2 (10), 685–694.
Hacker, C.D., et al., 2012. Resting state functional connectivity of the striatum in Parkinson's disease. Brain 135 (Pt 12), 3699–3711.
Hayasaka, S., Nichols, T.E., 2003. Validating cluster size inference: random field and permutation methods. Neuroimage 20 (4), 2343–2356.
He, B.J., et al., 2010. The temporal structures and functional significance of scale-free brain activity. Neuron 66 (3), 353–369.
Honey, C.J., et al., 2009. Predicting human resting-state functional connectivity from structural connectivity. Proc. Natl. Acad. Sci. U. S. A. 106 (6), 2035–2040.
Hormuzdi, S.G., et al., 2001. Impaired electrical signaling disrupts gamma frequency oscillations in connexin 36-deficient mice. Neuron 31 (3), 487–495.
Jinno, S., et al., 2007. Neuronal diversity in GABAergic long-range projections from the hippocampus. J. Neurosci. 27 (33), 8790–8804.
Kraft, A.W., et al., 2017. Visual experience sculpts whole-cortex spontaneous infraslow activity patterns through an Arc-dependent mechanism. Proc. Natl. Acad. Sci. U. S. A. 114 (46), E9952–E9961.

Laumann, T.O., et al., 2015. Functional system and areal organization of a highly sampled individual human brain. Neuron 87 (3), 657–670.
Lytton, W.W., Sejnowski, T.J., 1991. Simulations of cortical pyramidal neurons synchronized by inhibitory interneurons. J. Neurophysiol. 66 (3), 1059–1079.
Ma, Y., et al., 2016. Resting-state hemodynamics are spatiotemporally coupled to synchronized and symmetric neural activity in excitatory neurons. Proc. Natl. Acad. Sci. U. S. A. 113 (52), E8463–E8471.
Matsui, T., Murakami, T., Ohki, K., 2016. Transient neuronal coactivations embedded in globally propagating waves underlie resting-state functional connectivity. Proc. Natl. Acad. Sci. U. S. A. 113 (23), 6556–6561.
McKiernan, K.A., et al., 2003. A parametric manipulation of factors affecting task-induced deactivation in functional neuroimaging. J. Cognit. Neurosci. 15 (3), 394–408.
Murphy, K., Fox, M.D., 2017. Towards a consensus regarding global signal regression for resting state functional connectivity MRI. Neuroimage 154, 169–173.
Pawela, C.P., et al., 2008. Resting-state functional connectivity of the rat brain. Magn. Reson. Med. 59 (5), 1021–1029.
Picchioni, D., Duyn, J.H., Horovitz, S.G., 2013. Sleep and the functional connectome. Neuroimage 80, 387–396.
Postma, F., et al., 2011. Electrical synapses formed by connexin36 regulate inhibition- and experience-dependent plasticity. Proc. Natl. Acad. Sci. U. S. A. 108 (33), 13770–13775.
Power, J.D., et al., 2014. Methods to detect, characterize, and remove motion artifact in resting state fMRI. Neuroimage 84, 320–341.
Power, J.D., et al., 2011. Functional network organization of the human brain. Neuron 72 (4), 665–678.
Raichle, M.E., et al., 2001. A default mode of brain function. Proc. Natl. Acad. Sci. U. S. A. 98 (2), 676–682.
Shigematsu, N., Nishi, A., Fukuda, T., 2019. Gap junctions interconnect different subtypes of parvalbumin-positive interneurons in barrels and septa with connectivity unique to each subtype. Cerebr. Cortex 29 (4), 1414–1429.
Silasi, G., et al., 2016. Intact skull chronic windows for mesoscopic wide-field imaging in awake mice. J. Neurosci. Methods 267, 141–149.
Simpson, J.R., et al., 2000. The emotional modulation of cognitive processing: an fMRI study. J. Cognit. Neurosci. 12 (Suppl. 2), 157–170.
Simpson Jr., J.R., et al., 2001. Emotion-induced changes in human medial prefrontal cortex: I. During cognitive task performance. Proc. Natl. Acad. Sci. U. S. A. 98 (2), 683–687.
Somogyi, P., et al., 1998. Salient features of synaptic organisation in the cerebral cortex. Brain Res Brain Res Rev 26 (2–3), 113–135.
Sporns, O., 2013. Network attributes for segregation and integration in the human brain. Curr. Opin. Neurobiol. 23 (2), 162–171.
Stafford, J.M., et al., 2014. Large-scale topology and the default mode network in the mouse connectome. Proc. Natl. Acad. Sci. U. S. A. 111 (52), 18745–18750.
Tononi, G., Sporns, O., Edelman, G.M., 1994. A measure for brain complexity: relating functional segregation and integration in the nervous system. Proc. Natl. Acad. Sci. U. S. A. 91 (11), 5033–5037.
Vincent, J.L., et al., 2007. Intrinsic functional architecture in the anaesthetized monkey brain. Nature 447 (7140), 83–86.
Wang, Y., Belousov, A.B., 2011. Deletion of neuronal gap junction protein connexin 36 impairs hippocampal LTP. Neurosci. Lett. 502 (1), 30–32.
White, B.R., et al., 2011. Imaging of functional connectivity in the mouse brain. PLoS One 6 (1), e16322.
Whittington, M.A., Traub, R.D., Jefferys, J.G., 1995. Synchronized oscillations in interneuron networks driven by metabotropic glutamate receptor activation. Nature 373 (6515), 612–615.
Wright, P.W., et al., 2017. Functional connectivity structure of cortical calcium dynamics in anesthetized and awake mice. PLoS One 12 (10), e0185759.
Xie, Y., et al., 2016. Resolution of high-frequency mesoscale intracortical maps using the genetically encoded glutamate sensor iGluSnFR. J. Neurosci. 36 (4), 1261–1272.
Yan, C.G., et al., 2013. A comprehensive assessment of regional variation in the impact of head micromovements on functional connectomics. Neuroimage 76, 183–201.
Zhang, D., et al., 2008. Intrinsic functional relations between human cerebral cortex and thalamus. J. Neurophysiol. 100 (4), 1740–1748.
Zlomuzica, A., et al., 2012. Behavioral alterations and changes in Ca/calmodulin kinase II levels in the striatum of connexin36 deficient mice. Behav. Brain Res. 226 (1), 293–300.